Photoproduction of η mesons off neutrons from a deuteron target

A.V. Anisovich[1,2], I. Jaegle[3], E. Klempt[1], B. Krusche[3], V.A. Nikonov[1,2], A.V. Sarantsev[1,2], and U. Thoma[1]

[1] Helmholtz–Institut für Strahlen– und Kernphysik der Universität Bonn, Nußallee 14-16, 53115 Bonn, Germany
[2] Petersburg Nuclear Physics Institute, Gatchina, 188300 Russia
[3] Institut für Physik der Universität Basel, Klingelbergstrasse 82, CH-4056 Basel, Switzerland

Abstract. A formalism is developed for the partial wave analysis of data on meson photoproduction off deuterons and applied to photoproduction of η and π^0 mesons. Different interpretations of a dip-bump structure of the η photoproduction cross section in the 1670 MeV region are presented and discussed. Helicity amplitudes for two low-mass S_{11} states are determined.

PACS. 11.80.Et Partial-wave analysis – 13.30.-a Decays of baryons – 13.40.-f Electromagnetic processes and properties – 14.20.Gk Baryon resonances with S=0

1 Introduction

The cross section for photoproduction of η mesons off protons is dominated by the $N(1535)S_{11}$ resonance, other resonances make only minor contributions. In particular the $N(1650)S_{11}$ resonance, which one would naively expect to contribute to η photoproduction in a similar strength as $N(1535)S_{11}$, is hardly visible in the total cross section. There are two explanations why $N(1650)S_{11}$ is so much suppressed compared to $N(1535)S_{11}$: the $N(1650)S_{11} \to N\eta$ decay branching fraction is much smaller than that for $N(1535)S_{11}$ decays, and the $N(1650)S_{11}$ photoproduction cross section seems to be suppressed compared to $N(1535)S_{11}$ photoproduction.

The large $N(1535)S_{11} \to N\eta$ coupling found different interpretations by Isgur and Karl [1], by Weise and collaborators [2] and by Glozman and Riska [3]. In [1], the two quark-model S_{11} states with $s = 1/2$ and $s = 3/2$, respectively, have appreciable mixing (with a mixing angle of $-31°$). A phenomenological fit to baryon decays had given precisely this value [4]. For this mixing angle, $N(1650)S_{11}$ decouples from $N\eta$ decays while $N(1535)S_{11}$ has a strong coupling to $N\eta$. In [2], $N\eta$ and ΣK photoproduction were described by the dynamics of the coupled $\Sigma K - p\eta$-system; no genuine 3-quark resonance was required in their model. In [3], the $N(1535)S_{11}$ is a conventional 3-quark state; one-pion exchange was assumed to make an essential contribution to quark-quark interactions. Clustering of the baryonic wave functions into quarks and diquarks then led to the strong selectivity of the $N(1535)S_{11} \to N\eta$ coupling.

The Moorhouse rule [5] gives a second reason for the small η photoproduction cross section off protons. This selection rule forbids photo-excitations off protons of spin $3/2$ members of the lowest-mass $[70, 1^-]$ super-multiplet of nucleon resonances. The Moorhouse rule forbids only transitions to the $[70,^4 8]$ component of the $N(1650)S_{11}$. Burkert et al. [6] analyzed the existing photo- and electroproduction data and extracted transition amplitudes for transitions from the nucleon ground state to the $[70, 1^-]$ super-multiplet. The - scarce - data on electro-production off neutrons were not used; due to their large errors, the data at the photo-point hardly constrained their analysis.

Recently, photoproduction of η mesons off neutrons has attracted additional interest. A narrow structure at 1.67 GeV was observed which was not easily understood in terms of known nucleon excitations. It was first reported by the GRAAL collaboration at NSTAR2004 [7] and interpreted as narrow resonance by part of the authors [8,9]. The bump-like structure in the $n\eta$ invariant mass distribution is not seen in the cross section on the proton even though a reanalysis of the GRAAL data [10] indicated the possibility of a bump structure at 1.69 GeV also for proton data. This structure was suggested to signal the existence of a relatively narrow ($M \approx 1.68$ GeV, $\Gamma \leq 30$ MeV) baryon state. In particular the possibility that the state is the non-strange member of an anti-decuplet of pentaquarks [11,12,13] is an attractive possibility. The bump structure in the $n\eta$ invariant mass spectrum was confirmed by the CB-ELSA/TAPS [14] and LEPS [15] collaborations.

Different interpretations have been offered as origin of this structure. Choi et al. [16] use three known nucleon resonances, $N(1535)S_{11}$, $N(1650)S_{11}$ $N(1710)P_{11}$, and a nar-

Correspondence to: klempt@hiskp.uni-bonn.de

row state at 1675 MeV which they discuss as pentaquark $N(1675)P_{11}$. Vector meson exchange in the t channel was used as a background amplitude.

The Giessen group arrives at different conclusions [17]. Within their unitary coupled-channels effective Lagrangian approach, the cross section of η photoproduction on the neutron was fully described. The peak at $\sqrt{s}$=1.66 GeV was explained as coupled-channel effect due to $N(1650)S_{11}$ and $N(1710)P_{11}$ resonance excitations. No narrow resonance was required.

The analysis of Fix *et al.* [18] required, in addition to the conventional ingredients of the MAID model, a narrow state which was assumed to have P_{11} quantum numbers.

In this paper, we present a partial wave analysis of the recent data of the CB-ELSA/TAPS collaboration [19] on $\gamma d \to p_{\text{spectator}} n\eta$. In view of the long-standing discrepancies between the photo-production amplitude $A_{1/2}^n$ for $N(1535)S_{11}$ production ($A_{1/2}^n = -0.020 \pm 0.035\,\text{GeV}^{-1/2}$ from $\gamma n \to n\pi^0$ [20]; $A_{1/2}^n = -0.100 \pm 0.030\,\text{GeV}^{-1/2}$ from $\gamma n \to n\eta$ [21]), it seems adequate to include some older data on $\gamma n \to n\pi^0$, but we also include recent data from GRAAL on the beam asymmetry for $\gamma n \to n\eta$ [22] and $\gamma n \to n\pi^0$ [23]. In addition, we use data on photoproduction of $2\pi^0$, $\pi^0\eta$ and of hyperons as well as some partial-wave amplitudes from elastic πN scattering and data on $\pi^- p \to p2\pi^0$. A survey of the data used in the fits, of the partial wave analysis method and of recent results can be found elsewhere [24,25,26,27,28].

The paper is organized as follows: after this introduction we present, in section 2, how the Fermi motion of the neutron in the deuteron is treated. Reasonable consistency is found for the $\gamma p \to p\eta$ cross sections for protons bound in deuterons - folded with the Fermi momentum distribution - with the cross sections measured on free protons. The success encouraged us to perform a partial wave analysis for the part of the data where the proton acts as a spectator. The fits and the results are presented in section 3. The paper ends with a short summary and our conclusions (section 4).

2 Fermi motion

Experimentally, the cross section for η meson photoproduction off deuterons is measured. The deuteron is at rest in the laboratory system, the neutron not. It has had, at the moment of the interaction, the same (but opposite) momentum as the proton. A cut in the missing momentum of the (undetected) proton selects events in which the proton acted as spectator.

There are two approaches to fit data. First, one could unfold the experimentally observed cross section to determine the cross section for a neutron target. This data can then be fitted. Alternatively, the calculated cross section can be folded with the neutron momentum. In this way, adopted here, the fitted cross section can be compared directly to the measured quantities.

The differential cross section for production of n particles in the photon nucleon interaction has the form

$$d\sigma_{\gamma N} = \frac{(2\pi)^4 |A|^2}{4\sqrt{(k_1 k_2)^2 - m_1^2 m_2^2}}\, d\Phi_n(P, q_1, \ldots, q_n) \quad (1)$$

where k_i and m_i are the four–momenta and masses of the initial particles, P is the total momentum ($P = k_1 + k_2$) and q_i are the four–momenta of final state particles. The $d\Phi_n(P, q_1, \ldots, q_n)$ is the n-body phase volume

$$d\Phi_n(P, q_1, \ldots, q_n) = \delta^4(P - \sum_{i=1}^{n} q_i) \prod_{i=1}^{n} \frac{d^3 q_i}{(2\pi)^3 2q_{0i}} \quad (2)$$

where q_{0i} are the energy components.

In the case of meson photoproduction off nucleons bound in a deuteron, the cross section (1) should be integrated over its momentum:

$$d\sigma_{\gamma D} = \int d|\mathbf{p}_N|\, |\mathbf{p}_N|^2 f^2(|\mathbf{p}_N|) \frac{dz_N d\phi_N}{4\pi} \frac{(2\pi)^4 |A|^2}{4\sqrt{(k_1 p_N)^2}} \times$$
$$d\Phi_n(k_1 + p_N, q_1, \ldots, q_n), \quad (3)$$

where $\mathbf{p}_N$ is the momentum of the nucleon, $z_N = \cos\Theta_N$, and where $dz_N d\phi_N$ forms the solid angle element of the nucleon in the laboratory system. The function $f(P_N)$ describes the momentum distribution of the nucleon inside the deuteron. It can be chosen in the form of the Paris [29] or Gatchina wave function [30].

The spectator nucleon in the γd interaction has the momentum $p_s = -p_N$ in the lab system (deuteron at rest) and is on shell. Therefore the energy of the interacting particle is given by

$$E_N = M_d - \sqrt{m_s^2 + \mathbf{p}_N^2} \quad (4)$$

where M_d is the deuteron mass and m_s is the mass of the spectator nucleon. The off shell mass squared (t) of the interacting nucleon and the total energy squared in the γN interaction $s_{tot}(t)$ are equal to

$$t = E_N^2 - m_N^2 \qquad s_{tot}(t) = t + 2E_\gamma\big(\sqrt{\mathbf{p}_N^2 + t} - |\mathbf{p}_N|z_N\big).$$

A major problem in this approach is to relate the off-shell amplitude of the interacting particles with measurable on-shell distributions. It can be shown [21] that the best description is achieved under the assumption

$$\sigma(s_{tot}(t), t) = \sigma(s_{tot}(m_N^2), m_N^2)$$
$$\sigma(s_{tot}(t), t) = 0 \quad \text{for} \quad s_{tot}(t) < (m_N + m_\eta)^2. \quad (5)$$

Due to relation (5), all further calculations can be performed for an on-shell nucleon. The components of the initial 4-vectors in the lab system are defined as

$$p_N = (p_{0N}, p_{xN}, p_{yN}, p_{zN}) \quad k_1 = (E_\gamma, 0, 0, E_\gamma)$$
$$p_{xN} = |\mathbf{p}_N|\sin\Theta_N\cos\phi_N, \quad p_{zN} = |\mathbf{p}_N|z_N$$
$$p_{yN} = |\mathbf{p}_N|\sin\Theta_N\sin\phi_N, \quad p_{0N} = \sqrt{m_N^2 + \mathbf{p}_N^2} \quad (6)$$

where m_N is nucleon mass and momentum of the photon $\mathbf{k}_1$ is directed along z-axis.

In the case of single-meson photoproduction, the amplitude depends on the total energy of the γN system and the angle between the initial photon and the final meson calculated in the center of mass system (cms) of the reaction. Differential cross sections are usually given in the center of mass system of the photon and the hit nucleon. We will call this system as "data" system. Let us calculate the momentum of the particles and scattering angles in the laboratory system, in the cms and the "data" system.

The total energy squared (which is an invariant value) can be calculated, for example, in the laboratory system:

$$s_{tot} = (k_1 + p_N)^2 = m_N^2 + 2E_\gamma(p_{0N} - |\mathbf{p}_N|z_N). \quad (7)$$

Then in cms of the reaction:

$$z_{cms} = \frac{\mathbf{q}_1^{cms}\mathbf{k}_1^{cms}}{|\mathbf{q}_1^{cms}||\mathbf{k}_1^{cms}|} = \frac{q_{10}^{cms}k_{10}^{cms} - (q_1 k_1)}{|\mathbf{q}_1^{cms}||\mathbf{k}_1^{cms}|},$$

$$q_{10}^{cms} = \frac{s_{tot} + m_1^2 - m_N^2}{2\sqrt{s_{tot}}}, \quad k_{10}^{cms} = \frac{s_{tot} - m_N^2}{2\sqrt{s_{tot}}},$$

$$|\mathbf{q}_1^{cms}| = \sqrt{(q_{10}^{cms})^2 - m_1^2}, \qquad |\mathbf{k}_1^{cms}| = k_{10}^{cms}. \quad (8)$$

Here, q_1 is the 4-momentum of the final meson with mass m_1. The invariant quantity $(q_1 k_1)$ can be calculated in any system (e.g. the "data" system).

To define the photon 4-vector in the "data" system let us calculate the invariant $(k_1 P_{eff})$, where P_{eff} is the sum of photon and nucleon momenta, in both the laboratory system and in the "data" system.

$$P_{eff}^{lab} = (m_N + E_\gamma, 0, 0, E_\gamma), \quad k_1^{lab} = (E_\gamma, 0, 0, E_\gamma)$$

$$P_{eff}^{data} = (\sqrt{s_{eff}}, 0, 0, 0), \qquad k_1^{data} = (E_\gamma^m, 0, 0, E_\gamma^m). \quad (9)$$

Comparing this invariant in the two systems we obtain

$$E_\gamma^m = \frac{m_N E_\gamma}{\sqrt{s_{eff}}}, \qquad s_{eff} = m_N^2 + 2m_N E_\gamma \quad (10)$$

Then the invariant $(k_1 q_1)$ in the "data" system is equal to

$$q_1 k_1 = \frac{m_N E_\gamma}{\sqrt{s_{eff}}}(\sqrt{m_1^2 + |\mathbf{q}|^2} - |\mathbf{q}|\, z). \quad (11)$$

In this equation, $\mathbf{q}$ is the laboratory momentum of the meson. As a result, we can express all variables in terms of measured values; needed are - in the "data" system - the photon energy E_γ and z, the cosine of the angle between meson and photon.

Our next task is to define the initial nucleon momentum in the "data" system. Then:

$$p_N^m = (p_{0N}^m, p_{xN}, p_{yN}, p_{zN}^m)$$

$$p_{0N}^m = \frac{p_{0N} m_N + E_\gamma(p_{0N} - p_{zN})}{\sqrt{s_{eff}}},$$

$$p_{zN}^m = p_{0N}^m - (p_{0N} - p_{zN})\frac{\sqrt{s_{eff}}}{m_N} \quad (12)$$

The transition from the lab system to the "data" system is performed via a boost along the z-axis, so "x" and "y" components of 4-vector are not changed. The equations for p_{0N}^m and p_{zN}^m can be obtained from the invariance of the scalar products $(p_N P_{eff})$ and $(p_N k_1)$ calculated in the lab and "data" systems.

Now one can calculate the phase volume for the meson-nucleon final state in the "data" system:

$$d\Phi_n(k_1^m + p_N^m, q_1, q_2) = \frac{\delta(P_0^m - q_{01} - q_{02})\, d^3 q_1}{4(2\pi)^6 q_{10}q_{20}} \quad (13)$$

where

$$q_{01} = \sqrt{m_1^2 + |\mathbf{q}|^2} \qquad q_{02} = \sqrt{m_N^2 + |\mathbf{P}^m - \mathbf{q}|^2}$$

$$P^m = (p_{0N}^m + E_\gamma^m, p_{xN}, p_{yN}, p_{zN}^m + E_\gamma^m) \quad (14)$$

and m_1 is the mass of the final meson.

From energy conservation, the absolute value of the meson momentum in the "data" system is calculated to

$$|\mathbf{q}| = \frac{\Sigma\xi|\mathbf{P}^m| + P_0^m\sqrt{\Sigma^2 - m_1^2[(P_0^m)^2 - |\mathbf{P}^m|^2\xi]}}{(P_0^m)^2 - |\mathbf{P}^m|^2\xi^2} \quad (15)$$

where

$$\Sigma = \frac{1}{2}(s_{tot} + m_1^2 - m_N^2) \quad (16)$$

and ξ is the cosine of the angle between $\mathbf{P}^m$ and $\mathbf{q}_1$:

$$\xi = \frac{zP_z^m + |\mathbf{p}_N|\sqrt{1 - z_N^2}\sqrt{1 - z^2}cos(\phi_N - \phi)}{|\mathbf{P}^m|} \quad (17)$$

and where ϕ is the azimuthal angle of the final meson. Then the phase volume is given by

$$d\Phi_n(P^m, q_1, q_2) = \frac{1}{4(2\pi)^6}\frac{|\mathbf{q}|^2 dz d\phi}{|\mathbf{q}|P_0^m - |\mathbf{P}^m|\xi\sqrt{m_1^2 + |\mathbf{q}|^2}}. \quad (18)$$

All variables now depend only on the relative angle $\phi_N - \phi$. In the evaluation of the cross section (3), one integration can be performed trivially and eq. (3) can be rewritten in the form

$$d\sigma_{\gamma D} = \int d|\mathbf{p}_N|\, |\mathbf{p}_N|^2 f^2(|\mathbf{p}_N|)\frac{dz_N d\phi_N}{4\pi} \times$$

$$\frac{|A(s_{tot}, z_{cms})|^2}{32\pi\,(k_1 p_N)}\frac{|\mathbf{q}|^2 dz}{|\mathbf{q}|P_0^m - |\mathbf{P}^m|\xi\sqrt{m_1^2 + |\mathbf{q}|^2}} \quad (19)$$

where

$$\xi = \frac{zP_z^m + |\mathbf{p}_N|\sqrt{1 - z_N^2}\sqrt{1 - z^2}cos(\phi_N)}{|\mathbf{P}^m|}$$

$$P_0^m = \frac{(p_{0N} + E_\gamma)m_N + E_\gamma(p_{0N} - p_{Nz})}{\sqrt{s_{eff}}}$$

$$|\mathbf{P}^m| = \frac{m_N(p_{zN} + E_\gamma) - E_\gamma(p_{0N} - p_{zN})}{\sqrt{s_{eff}}} + E_\gamma \quad (20)$$

and $|\mathbf{q}|$ is defined by eq.(15).

At low energies, the phase volume given by eq.(18) decreases for forward angles leading to a corresponding behavior of the cross section in the region where the S_{11} wave is the dominant contribution.

3 Photoproduction of η-mesons off deuterons

3.1 η photoproduction off protons

As a first step, we describe η photoproduction off protons bound in a deuteron. This allows us to test the reliability of the folding procedure accounting for the Fermi motion. The total cross section and the angular distributions are presented in Figs.1 and 2 for the case of the Paris wave function. The error bars on these figures represent statistical errors only.

For the fits, we use alternatively the Paris wave function [29] or a deuteron wave function obtained from a dispersion N/D-method [30]. The fit uses no new parameters: all masses, widths, partial decay widths, and helicity amplitudes are determined by the data from $\gamma p \to p\eta$ [31] and the fits described in [26]. The χ^2 was found to be 2396 for 380 points using the Paris wave function and 2410 with the N/D-based wave function. The χ^2's are similar demonstrating that the extraction of cross section from deuteron data is insensitive to details of the deuteron wave function. This observation is confirmed when cross sections for $\gamma n \to n\eta$ are extracted. Hence we show here only figures obtained by using the Paris wave function. The χ^2's are large; inspecting the differential cross sections and the deviations between data and fit suggests that systematic errors in the extraction of the cross sections may be responsible for a significant fraction of the large χ^2's.
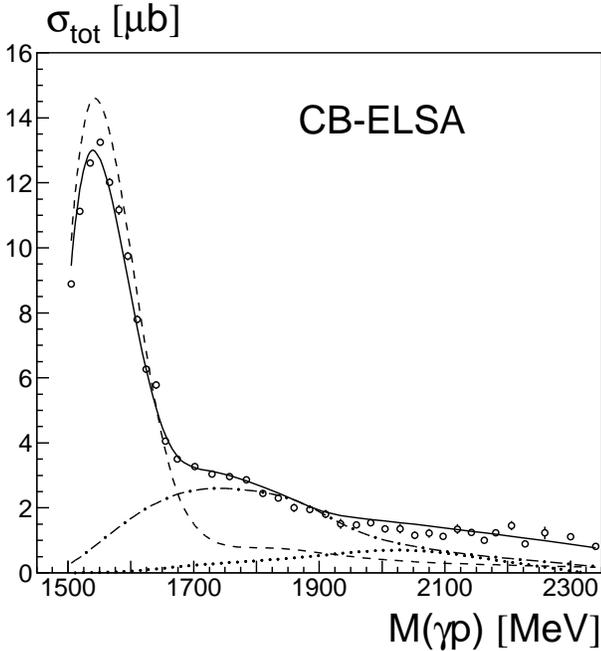
Fig. 1. The total cross section for $\gamma p \to \eta p$ from the deuteron target. The description of the data (solid line) is obtained from the solution on the free proton smeared with the Paris wave function. The dashed line is the S_{11}, the dash-dotted line the P_{13}, and the dotted line the D_{15} contribution.
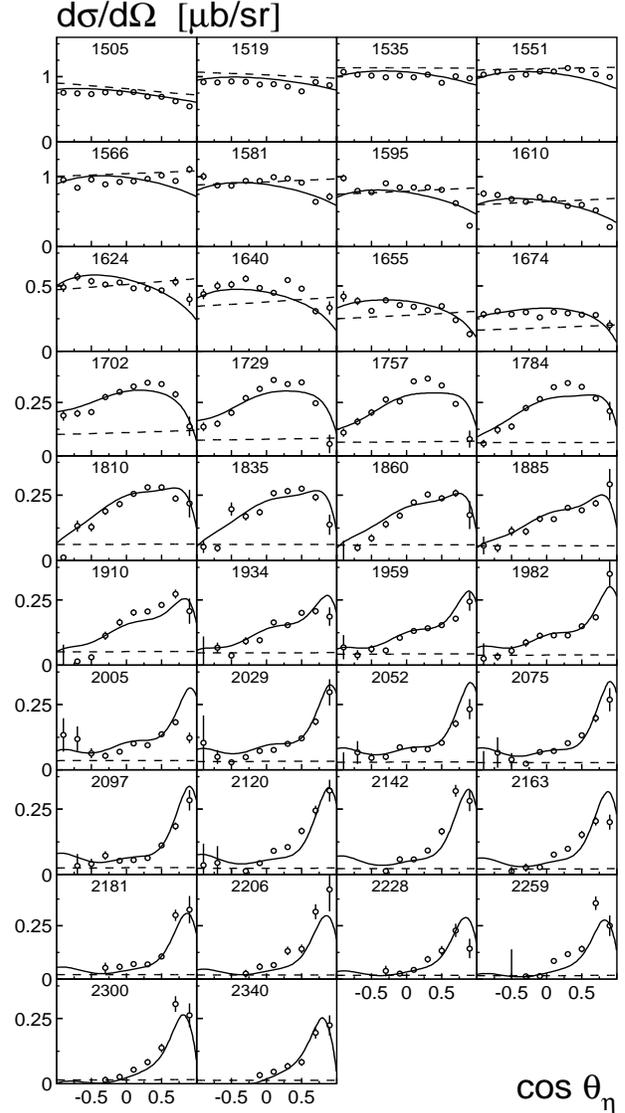
Fig. 2. The differential cross section for $\gamma p \to \eta p$ from the deuteron target in the 1505-2340 MeV mass range. The solid curves represent a fit to free-proton data smeared with the Paris wave function. The dashed curves show the contribution of the S_{11} wave.

3.2 The η and π photoproduction off neutrons

In the present analysis, the following data sets are added to our data base used in our fits: η photoproduction off the neutron from the CB-ELSA experiment [19], beam asymmetry for η [22] and π [23] photoproduction off the neutron from the GRAAL experiment and π photoproduction off the neutron from the SAID database [32]. These data were fitted together with other photo- and pion-induced single and double photoproduction data as listed in the Introduction. All our fits produced a very similar χ^2 for the Paris and N/D-based wave function. Hence we discuss only the investigations which had been done using the Paris wave functions.

dσ/dΩ [μb/sr]
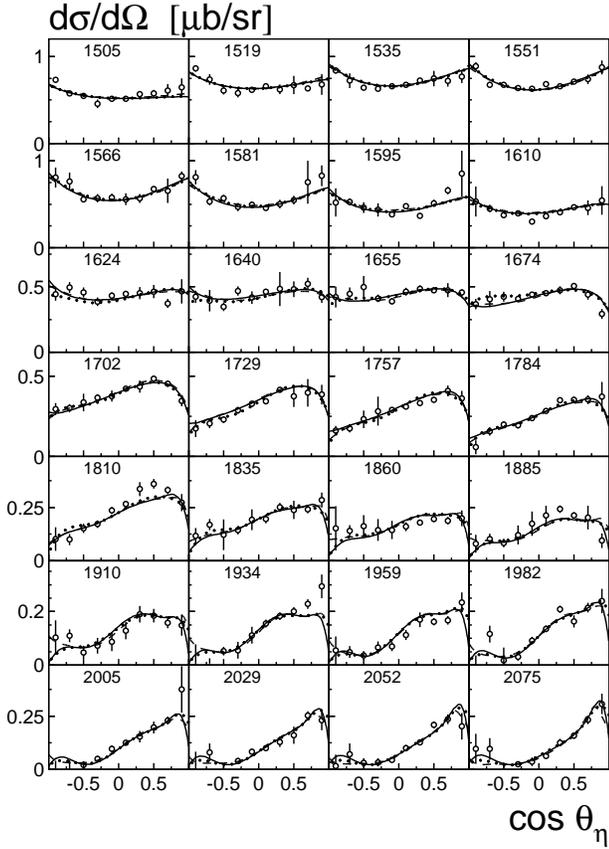
Fig. 3. The differential cross section for $\gamma n \to \eta n$ off deuterons [19]. The PWA description is shown as solid line (solution 1), dashed line (solution 2) and dotted line (solution 3).

Σ
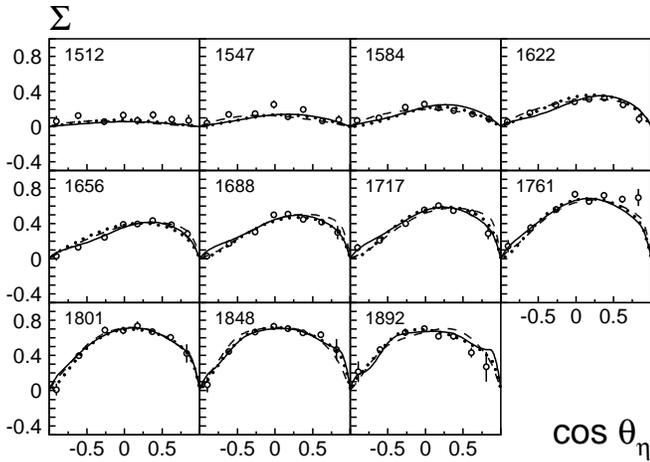
Fig. 4. Beam asymmetry for $\gamma n \to \eta n$ for neutrons bound in a deuteron [22]. The PWA description is shown as solid line (solutions 1), dashed line (solution 2), and dotted line (solution 3).

The differential cross section for $\gamma n \to n\eta$ is shown in Fig. 3, the beam asymmetry in Fig. 4. The corresponding data for $\gamma n \to \pi^0 n$ are shown in Fig. 5 and 6. The data are fitted using three different scenarios. In all cases, the most significant contributions came from the S_{11}, P_{11}, and P_{13} partial waves, with S_{11} providing the largest contribution.

dσ/dΩ [μb/sr]
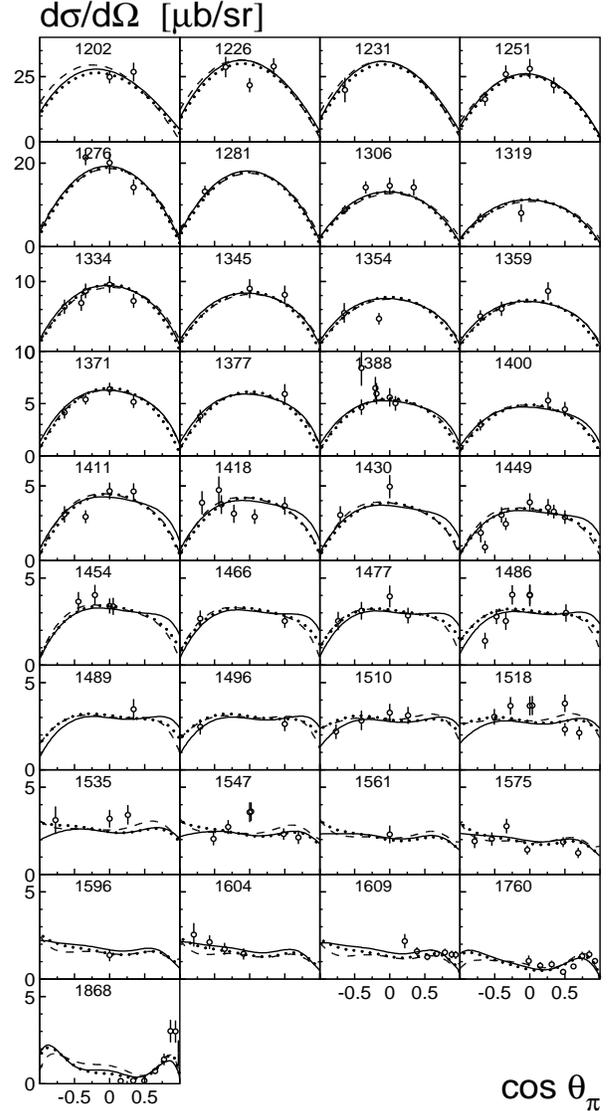
Fig. 5. The differential cross section for $\gamma n \to \pi^0 n$ using a deuteron target [32]. The PWA description is shown as solid line (solutions 1) , dashed line (solution 2), and dotted line (solution 3).

These three partial waves, and for the waves P_{33} and D_{33} which are irrelevant here, were described using K-matrices. For the other less important waves, relativistic multi-channel Breit-Wigner amplitudes were used. For the important waves, the elastic scattering amplitudes from [33] were included in the fit using the same K-matrix as for the photoproduction data.

In the first solution, the low-energy region is described mainly by the interference between $N(1535)S_{11}$ and $N(1650)S_{11}$. In the second solution we enforce a large contribution from a standard $N(1710)P_{11}$ resonance. In the third solution, we test the possibility of a narrow (less than 10 MeV) state at about 1650 MeV. The resulting fit curves are also shown in Figs. 3-6. In Table 1 we give a
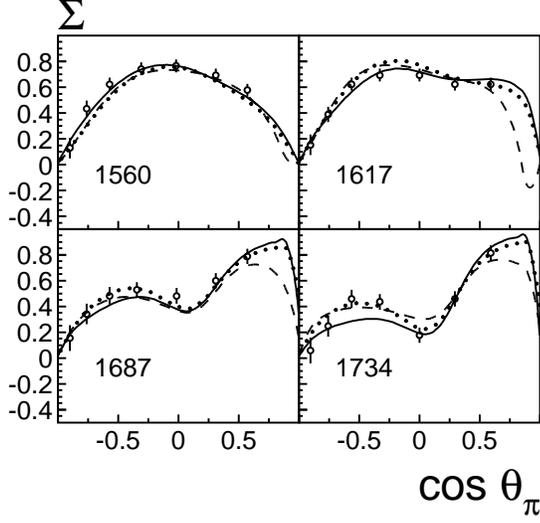
Fig. 6. Beam asymmetry for the reaction $\gamma n \to \pi^0 n$ from the deuteron target [23]. The PWA description is shown as solid line (solutions 1), dashed line (solution 2), and dotted line (solution 3).

breakdown of the χ^2 contributions of the four data sets in the three scenarios. All three scenarios provide an adequate description of the dip-bump structure observed in the $\gamma n \to n\eta$ total cross section.

A first analysis [38] of the preliminary CB-ELSA data [14] presented at NSTAR 2007 did not include t and u-exchanges due to the fact that in the low energy region these contributions are difficult to separate from other non-resonant terms. The present analysis is extended up to 2.1 GeV, first without contributions from t and u channel exchanges and second with these contributions included. The fits with t and u exchanges result in a slightly better description of the high energy tail but qualitatively do not change the solutions in the region below 1.75 GeV. However, both, the inclusion of t and u channel exchanges and the use of the final data decreased the helicity amplitudes. The new values reported here supersede those reported at NSTAR 2007. The contributions of high mass states are ambiguous and cannot be identified reliably. More data and further systematical investigations are needed. These uncertainties do not affect our conclusions concerning the low-mass region which is the prime issue of the study.

Table 1. Single meson photoproduction off neutron data used in the partial wave analysis and χ^2 for solutions 1 (interference in S_{11} wave), 2 ($N(1710)P_{11}$), and 3 (narrow P_{11}).

Observable	N_{data}	$\frac{\chi^2}{N_{\mathrm{data}}}$	$\frac{\chi^2}{N_{\mathrm{data}}}$	$\frac{\chi^2}{N_{\mathrm{data}}}$	Ref.
		Sol. 1	Sol. 2	Sol. 3	
$\sigma(\gamma n \to n\eta)$	280	1.32	1.26	1.31	[19]
$\Sigma(\gamma n \to n\eta)$	88	1.75	1.85	1.79	[22]
$\sigma(\gamma n \to n\pi^0)$	147	2.01	2.35	2.03	[32]
$\Sigma(\gamma n \to n\pi^0)$	28	1.02	1.07	0.90	[23]

3.2.1 Parameterization of the S_{11} wave

Following our previous analyses [31],[24] the S_{11} wave was parameterized as two pole, 5 channel K-matrix amplitude:

$$K_{ab} = \sum_{\alpha=1}^{2} \frac{g_a^{(\alpha)} g_b^{(\alpha)}}{M_\alpha^2 - s} + f_{ab}, \qquad (21)$$

where $a, b = p\pi,\, p\eta,\, K\Lambda,\, K\Sigma,\, \Delta\pi$, and M_α and $g_a^{(\alpha)}$ are masses and coupling constants of the K-matrix poles.

In [34] the non-resonant contributions were parameterized as linear mass dependent functions. We also found that such mass dependence introduced for the $\pi N \to \pi N$ and $\pi N \to \eta N$ and $\eta N \to \eta N$ non-resonant terms improves notably the description of the pion induced and photoproduction reactions. However, in our parameterization we introduced in addition a factor which suppresses the divergency of the non-resonant terms at large energies. Thus

$$f_{ab} = (f_{ab}^{(1)} + f_{ab}^{(2)}\sqrt{s})\frac{2 + s_{ab}}{s + s_{ab}} \qquad a, b = \pi N, \eta N \quad (22)$$

and $s_{ab} > 0$. The non-resonant transitions between $\pi N \to K\Lambda$, $\pi N \to K\Sigma$ and $\pi N \to \Delta\pi$ channels also improve the combined description. However these terms can be parameterized as constants. All other transitions contribute very little to the data description and were fixed to zero.

The amplitude for the transition between K-matrix channels can be written as:

$$A_{ab} = \hat{K}_{ac} \left(\hat{I} - i\hat{\rho}\hat{K}\right)^{-1}_{cb}. \qquad (23)$$

The phase space $\hat{\rho}$ is a diagonal matrix $\rho_{ab} = \delta_{ab}\,\rho_a$ with

$$\rho_a(s) = \frac{2|\mathbf{k}_B|}{\sqrt{s}} \frac{m_B^a + \sqrt{(m_B^a)^2 + |\mathbf{k}_B|^2}}{2m_B^a} \qquad (24)$$

for the two body final states. Here m_B^a is the mass and $\mathbf{k}_B$ is the momentum (calculated in the c.m.s. of the reaction) of the baryon in the channel (a) (see [35]). The parameterization of the $\Delta\pi$ phase volume is given in details in [35].

The K-matrix parameters for the πN and ηN channels are constrained from the fit of the elastic $\pi N \to \pi N$ data (extracted by [33]) and the fit of the $\pi^- p \to \eta n$ differential cross section [36],[37]. The description of these data is shown in Figs. 7 and 8.

The photoproduction amplitude is parameterized in the P–vector approach since the γN couplings are weak and do not contribute to rescattering. The amplitude is then given by

$$A_a = \hat{P}_b \left(\hat{I} - i\hat{\rho}\hat{K}\right)^{-1}_{ba}. \qquad (25)$$

with P-vector parameterized as:

$$P_b = \sum_\alpha \frac{g_{\gamma N}^{(\alpha)} g_b^{(\alpha)}}{M_\alpha^2 - s} + \tilde{f}_b \qquad (26)$$

Here $g_{\gamma N}^{(\alpha)}$ are γN couplings of the K-matrix poles and $\tilde{f}_b$ are non–resonant production terms, parameterized in the fit as real constants.
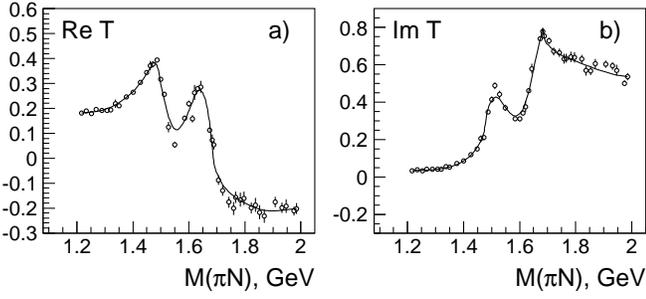
Fig. 7. The description of the $\pi N \to \pi N$ S_{11} amplitude obtained in the combined solution. The data are taken from energy independent solution [33].
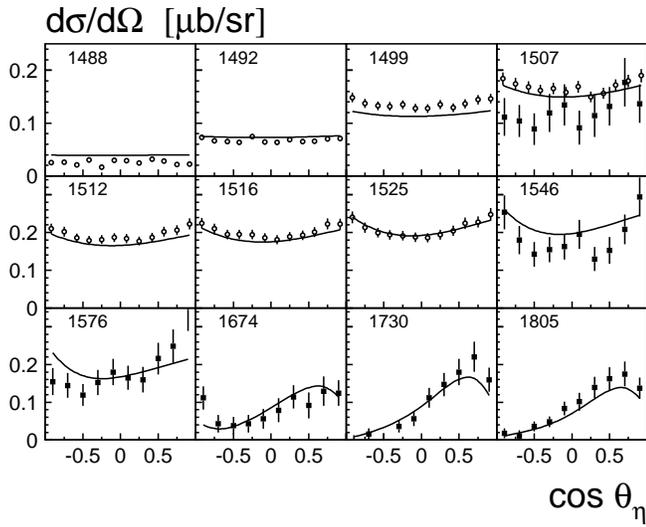
Fig. 8. The description of the $\pi p \to \eta n$ differential cross section obtained in the combined solution. The data are taken from [36] (open circles) and [37] (full squares).

Fig. 9. The total cross section for the reaction $\gamma n \to \eta n$ from the deuteron target [19]. The PWA description from Solution 1 (Paris wave function) is shown as the solid line. The dashed line is the S_{11} contribution, dash-dotted line is P_{11} contribution and dotted line is P_{13} contribution The grey (online: green) curves show the corresponding cross sections on the free neutron (no Fermi motion)

3.2.2 Interference in the S_{11} wave

The first solution with a strong interference in the S_{11} wave provides a very good description of the fitted data (see Table 1). In particular the bump in the 1650 MeV region is well described. This solution gives the following helicity couplings for S_{11} resonances calculated at the pole positions of the S_{11} amplitude:

$$S_{11}(1535): \ A_{1/2}^n = -0.080 \pm 0.020 \ , \ \ \phi = 12° \pm 10°$$
$$S_{11}(1650): \ A_{1/2}^n = -0.060 \pm 0.015 \ , \ \ \phi = 40° \pm 25° \quad (27)$$

The bump in the region of 1650 MeV appears due to an interference between $S_{11}(1535)$, $S_{11}(1650)$ and a non-resonant background. In our combined solution of the single photoproduction data $S_{11}(1650)$ has the rather small (15%) branching ratio into the ηN channel. Therefore an appreciable large coupling of this state to the γn channel is needed to describe the bump structure. Here we are in contradiction with the Giessen result [17] where the bump appears with decreasing of the $S_{11}(1650)$ γn helicity coupling. The two S_{11} states have very close (apart from overall sign) couplings into γp and γn channels. However

there is an important correlation: the phase difference between the couplings is fixed more precise than the absolute numbers. We found the phase difference 5 ± 5 degrees for the γp channel and 28 ± 8 for the γn channel. The bump structure in the 1650-1700 MeV region becomes much less pronounced in the case of a smaller phase difference (see solutions discussed below).

The K-matrix parameters of the S_{11} wave are rather firmly fixed from the fit of the elastic data and photoproduction reactions off the proton. The only mandatory parameters to fit γn reactions are two P-vector γn pole couplings and five non-resonant production constants. The $\gamma n \to \pi n$ and $\gamma n \to \eta n$ can be fixed directly from the combined analysis of the differential cross sections and beam asymmetry data from the neutron target. Fixing these parameters to zero leads to a large deterioration of the combined description.

Among other non-resonant contributions the most important one is the direct production of the $K\Lambda$ channel. It can notably influence the structure at 1650-1700 MeV which is situated in vicinity of the $K\Lambda$ threshold. The $K\Sigma$ production only slightly improves the description at high energies and $\Delta\pi$ can be put to zero.

To check the influence of the $\gamma n \to K\Lambda$ and $\gamma n \to K\Sigma$ direct production terms we performed the fit fixing these parameters to zero value. To reproduce the description of the $\gamma n \to \eta n$ data we increase the weight of this data set by a factor of 2. In this fit we could reproduce the unpolarized ηn cross section and beam asymmetries for $\pi^0 n$

σ_{tot} [μb]

CB-ELSA

M(γn) [MeV]
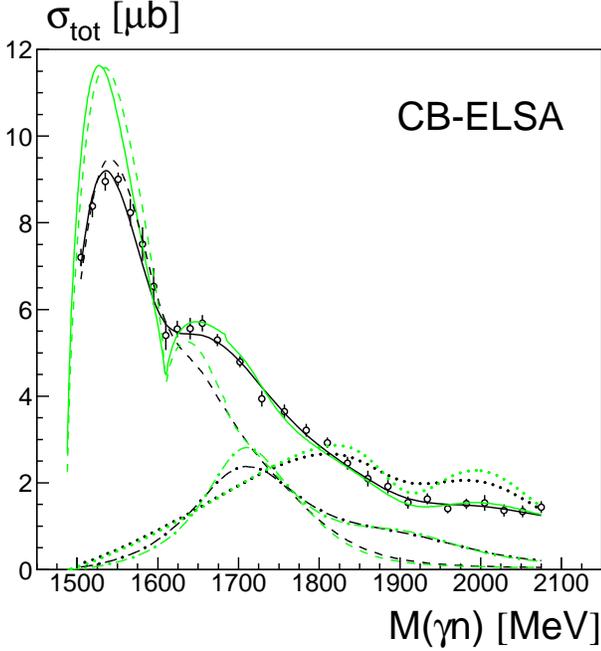
Fig. 10. The total cross section for the reaction $\gamma n \rightarrow \eta n$ from the deuteron target [19]. The PWA description from Solution 2 (Paris wave function) is shown as the solid line. The dashed line is the S_{11} contribution, dash-dotted line is P_{11} contribution and dotted line is P_{13} contribution The grey (online: green) curves show the corresponding cross sections on the free neutron (no Fermi motion)

and ηn. However the fit failed to reproduce the unpolarized $\gamma n \rightarrow \pi^0 n$ differential cross section: the χ^2 changed from 2.11 to 2.71. The residue for the $S_{11}(1535)$ state did not change within errors (27). The helicity coupling of the $S_{11}(1650)$ is slightly bigger in this solution: ~ 0.090 GeV$^{-\frac{1}{2}}$ and the phase difference with the first pole coupling reached 120 degrees.

A simplified parameterization provides a simplified picture: the difference in phases of helicity couplings in the γp and γn reactions is clearly seen. However it failed to describe simultaneously all reactions. This is one of the main reasons why analyses of different sets of photoproduction data results in incompatible helicity couplings.

The P_{11} and P_{13} waves provide contributions of similar strengths to $n\eta$. In the 1700 MeV region, the $N(1710)P_{11}$ resonance is weak while $N(1720)P_{13}$ makes a small contribution. The P_{11} wave becomes stronger at 1900 MeV.

3.2.3 Enforcing $N(1710)P_{11}$ contributions

We have investigated other mechanisms for an explanation of the bump-like structure in the region 1670 MeV. To prevent a strong interference in the S_{11} wave we forbid a direct photoproduction of the second K-matrix pole by setting its γn coupling to zero. We still observed some small interference effect in the S_{11} wave on the free neutron but it is too small to describe the bump-like structure in the data (see dashed lines in Fig. 10).

In some analyses, $N(1710)P_{11}$ has a sizable coupling to $N\eta$, the Review of Particle Properties calculates a branching ratio $Br(N(1710) \rightarrow N\eta) = (6.2 \pm 1.0)\%$. Indeed, with suppressed interference in the S_{11} wave and absence of an exotic state, this is the only mechanism which can explain the data. The χ^2 of the fit is very similar to the solution 1.

The contributions are depicted in Fig. 10. The helicity couplings for the S_{11} resonances calculated as residues in the pole position are determined to

$$S_{11}(1535): \ A_{1/2}^n = -0.080 \pm 0.020 \ , \ \ \phi = 10° \pm 10°$$
$$S_{11}(1650): \ A_{1/2}^n = -0.020 \pm 0.015 \ , \ \ \phi = 25° \pm 20° \quad (28)$$

This solution differs from the solution 1 by a different partial wave decomposition: it has a significant contribution from P_{11} in the region around 1.7 GeV which comes from the $N(1710)P_{11}$ resonance. The description of the total cross section for the Paris wave function is shown in Fig. 10. This analysis shows that there is a second possible mechanism to describe the existing experimental data and the structure around 1.67 GeV in η photoproduction.

As before, the dominant contribution stems from the S_{11} wave but in the 1700 MeV region, the P_{11} wave provides an appreciable contribution, too. In this solution, interference between $N(1535)S_{11}$ and $N(1650)S_{11}$ makes a visible but small effect.

σ_{tot} [μb]

CB-ELSA

M(γn) [MeV]
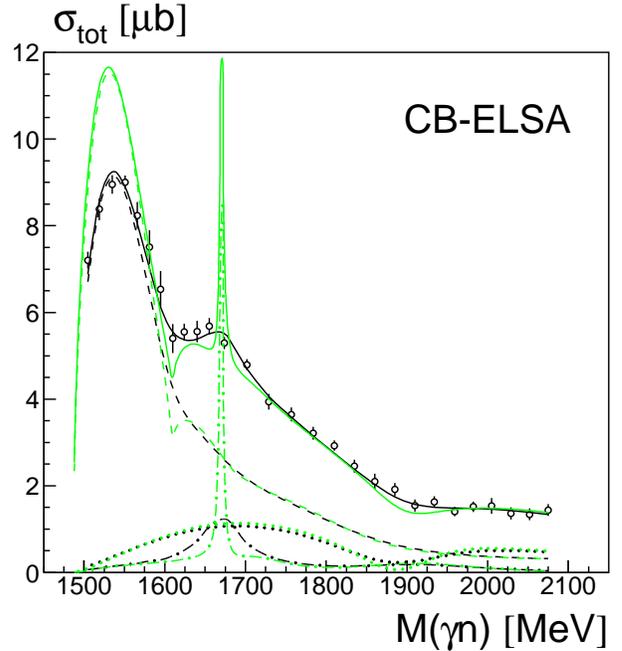
Fig. 11. The total cross section for the reaction $\gamma n \rightarrow \eta n$ from the deuteron target. The PWA description from Solution 3 (Paris wave function) is shown as the black solid line and the contributions as the colored solid lines. The dashed curves show the corresponding cross sections on the free neutron (no Fermi motion)

3.2.4 Is there a narrow P_{11} state?

A narrow P_{11} state in the region of 1670 MeV is discussed as a candidate for the pentaquark [41] and is one of the main motivations behind this analysis. In a third fit, we followed the procedure for the solution 2 but introduced a narrow state in the region 1670 MeV. Its mass optimized at 1670 ± 6 MeV. If its width was allowed to vary, the resonance became broader and interfered with the standard $N(1710)P_{11}$ resonance. The fits became unstable and a series of solutions were obtained in which a relatively narrow state and the broader $N(1710)P_{11}$ interfered. Solution 3, presented in the Fig. 11, shows the extreme where the broad $N(1710)P_{11}$ wave is absent. In this solution, the helicity coupling for the narrow P_{11} state is equal to $0.016\,\mathrm{GeV}^{-1/2}$, assuming a ηp branching to be 50%. It is interesting to note that Azimov *et al.* [42,41] derived a value $0.021\,\mathrm{GeV}^{-1/2}$ using the GRAAL data on η photoproduction off neutrons.

For the two S_{11} resonances the following helicity couplings are calculated:

$$S_{11}(1535): \; A_{1/2}^n = -0.076 \pm 0.015 \;, \;\; \phi = 25° \pm 10°$$
$$S_{11}(1650): \; A_{1/2}^n = -0.054 \pm 0.015 \;, \;\; \phi = 20° \pm 20° \quad (29)$$

3.3 η photoproduction on the free proton

Finally we consider the recent conjecture of Kuznetsov et al. [10] that the beam asymmetry for η photoproduction on free protons may reveal a structure in the 1.69 GeV region. Here, we check the compatibility of this data with solution 1 (interference in S_{11} wave) and/or with solution 3 (narrow P_{11}). In addition to [10] we include also the beam asymmetry data for η photoproduction from GRAAL [43].
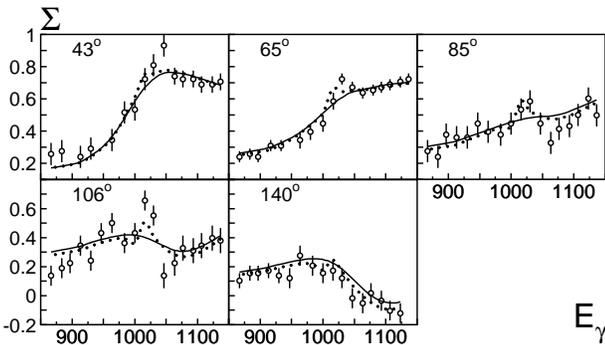
Fig. 12. Beam asymmetry for the reaction $\gamma p \to \eta p$ [10]. The PWA description is shown as solid line (solutions 1) and dotted line (solution 3).

The data on $\gamma p \to p\eta$ and fit are shown on Figs. 12 and 13. The data are described by the solution 1 with $\chi^2/N_{data} = 1.35$ (new data [10]) and $\chi^2/N_{data} = 1.85$ (GRAAL data [43]). Introducing a narrow P_{11} state (solution 3) results in a $\chi^2/N_{data} = 0.95$ (new data [10]) and
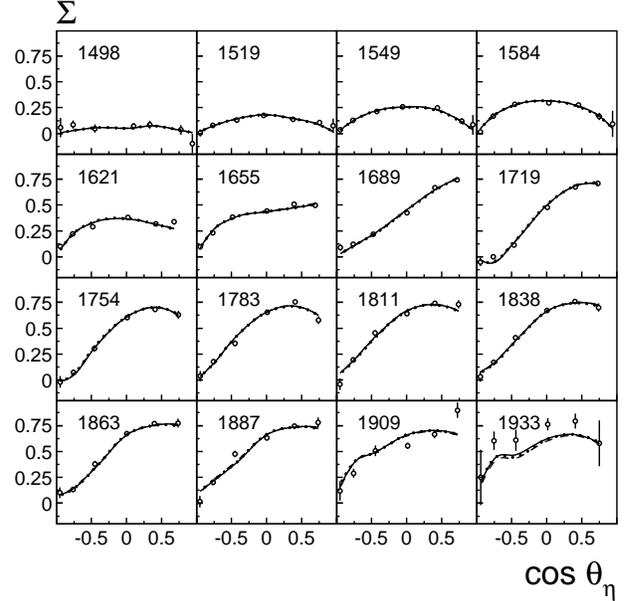
Fig. 13. Beam asymmetry for the reaction $\gamma p \to \eta p$ [43]. The PWA description is shown as solid line (solutions 1) and dotted line (solution 3).

$\chi^2/N_{data} = 1.90$ (GRAAL data [43]). Although the solution with a narrow P_{11} gives a better description of the new data [10], the fit faces some problems. While all individual pictures in Fig. 13 exhibit a peak-like structures, they cannot be described consistently by one resonance with one unique mass position. Hence new high precision data on this reactions are urgently needed if this idea is to be pursued further.

3.4 Helicity amplitudes

Main parameters for the two S_{11} states are given in Table 2. Pole positions and photoproduction couplings off protons are in good agreement with a previous analysis [24]. The main change was found in the imaginary part of the pole positions: the first pole of the S_{11} amplitude became a bit narrower and the second pole a bit broader. Both resonances have a Flatte like structure, the first one due to the ηN threshold and the second one due to $K\Lambda$. In Table 2, the position of the poles closest to the physical region are listed. The behavior of the Flatte amplitude is defined by an interplay of two poles on two sheets defined by the cut; small instabilities in pole positions are hence not surprising.

The helicity couplings given in Table 2 are calculated as the residues at the pole position and have phases. For protons, our $N(1535)S_{11}$ helicity amplitude coincides with the PDG estimate, for neutrons the two errors just cover the difference [44]. The discrepancy is due to the results reported in [20,45] while most analyses [21,46,47,48] quote values which are fully compatible with our finding.

For the $N(1650)S_{11}$, we found stronger photon couplings than the average value given in [44], with the differences being at the 2σ level. We point out that our values

provide a consistent description of almost all existing data sets. Our γn coupling is, for the first time, derived from η photoproduction off neutrons (and constrained by π^0 photoproduction off neutrons).

The values in Table 2 are averaged using the first and third solution. In the solution proposing a large $P_{11}(1710)$ contribution, the γn coupling of the $N(1650)S_{11}$ was found ~ 0.4 times smaller (see (28)).

We have not found other mechanisms to describe the bump structure in the region 1700 MeV. An explanation given in [49] as a possible contribution from $D_{15}(1675)$ is ruled out by our analysis. The combined fit to the π, η photoproduction off free protons and the deuteron and the results from the elastic πN scattering fixes well the branching ratio to the ηN channel (which is $< 6\%$) and helicity couplings. Although there is a rather large error for the γn coupling of the $D_{15}(1675)$ resonance, we could only reach a contribution of $0.5\,\mu$b from this state to the $\gamma n \to \eta n$ total cross section which is far from the value needed for a good description of the data.

Finally, we note that we do not use different helicity amplitudes for π and η photoproduction. Discrepancies, as found in the literature for both S_{11} resonances, between helicity amplitudes derived from different data cannot occur.

In the so-called "Single Quark Transition Model", Burkert *el al.* [6] extracted amplitudes for electromagnetic transitions from proton and neutron to excited states. The extrapolation to the photon point (read off their diagrams) are listed in Table 3. The agreement is excellent.

Finally we also compare our photocouplings with model calculations [50,51,52,53]. In all models, the signs are right and the magnitudes agree with the experimental values at the 30% level. On the basis of this data, no preference can be given to one particular model calculation.

4 Conclusions

We have presented an analysis of data on photoproduction of η (and π^0) mesons off neutrons. The analysis was

Table 2. Masses and widths (in GeV) and helicity amplitudes of $S_{11}(1535)$ and $S_{11}(1650)$.

	$S_{11}(1535)$	$S_{11}(1650)$
Pole position (mass)	1.505 ± 0.020	1.640 ± 0.015
(width)	0.145 ± 0.025	0.165 ± 0.015
PDG	1.510 ± 0.020	1.655 ± 0.015
	0.170 ± 0.080	0.165 ± 0.015
$A^p_{1/2}$ (GeV$^{-1/2}$)	0.090 ± 0.025	0.100 ± 0.035
PDG	0.090 ± 0.030	0.053 ± 0.016
phase	$(20 \pm 15)^\circ$	$(25 \pm 20)^\circ$
$A^n_{1/2}$ (GeV$^{-1/2}$)	-0.080 ± 0.020	-0.055 ± 0.020
PDG	-0.046 ± 0.027	-0.015 ± 0.021
phase	$(20 \pm 20)^\circ$	$(30 \pm 25)^\circ$

Table 3. Model predictions of $S_{11}(1535)$ and $S_{11}(1650)$ helicity amplitudes for protons and neutrons (in 10^{-3}GeV$^{-1/2}$).

		This work	[6]	[50]	[51]	[52]	[53]
N_{1535}	p	90 ± 25	97	+147	+142	+127	+76
	n	-80 ± 20	-53	-119	-77	-103	-63
N_{1650}	p	100 ± 35	90	+88	+78	+91	+54
	n	-55 ± 20	-32	-35	-47	-41	-35

motivated by a bump structure at 1670 MeV observed in the total cross section for $\gamma n \to n\eta$ in several experiments. There is a hot discussion in the literature if the structure signals a resonance. Often, it is interpreted as evidence for a pentaquark with hidden strangeness.

We find that the data can naturally be interpreted by interference within the S_{11} wave. This is the most natural interpretation and does not require any ad-hoc assumption. Other interpretations can, however, not be ruled out. The $N(1650)S_{11}$ may have a small coupling to $n\gamma$. Then, the P_{11} amplitude plays a more significant role. For an appropriate choice of parameters, a narrow P_{11} can be introduced and the data are well described. Hence the data do not support the need to introduce a narrow resonance but, for a suited set of parameters, the existence of a narrow resonance is also not ruled out. Fluctuations in recent beam asymmetry data for $\gamma p \to p\eta$ may serve as an indication for a narrow structure at 1670 MeV but fits without it provide a reasonable description of the data as well.

A second aspect of the data is the determination of helicity amplitudes. Our values are mostly consistent with those listed by the Particle Data Group. Comparison with model calculations show reasonable agreement but none of the models gives strikingly better results than the other models. Our values agree very well with a fit to electroproduction data using the "Single Quark Transition Model", Burkert *el al.* [6].

References

1. N. Isgur and G. Karl, Phys. Lett. **72B** (1977) 109.
2. N. Kaiser *et al.*, Phys. Lett. **B362** (1995) 23.
3. L.Y. Glozman, D.O. Riska, Phys. Lett. **B366** (1996) 305.
4. A. J. G. Hey, P. J. Litchfield and R. J. Cashmore, Nucl. Phys. B **95** (1975) 516.
5. R. G. Moorhouse, Phys. Rev. Lett. **16**, 772 (1966).

6. V. D. Burkert, R. De Vita, M. Battaglieri, M. Ripani and V. Mokeev, Phys. Rev. C **67** (2003) 035204.

7. V. Kuznetsov *et al.*, [GRAAL Collaboration], Workshop on the Physics of Excited Nucleons (NSTAR 2004), Grenoble, France, 24-27 Mar 2004, arXiv:hep-ex/0409032.

8. V. Kuznetsov *et al.*,, "Evidence for a narrow structure at W approx. 1.68-GeV in eta photoproduction on the neutron", unpublished, arXiv:hep-ex/0606065.

9. V. Kuznetsov *et al.*, Phys. Lett. B **647** (2007) 23.

10. V. Kuznetsov, M. Polyakov, T. Boiko, J. Jang, A. Kim, W. Kim and A. Ni, Acta Phys. Polon. **39** (2008) 1949.

11. D. Diakonov, V. Petrov and M. V. Polyakov, Z. Phys. A **359**, 305 (1997) [arXiv:hep-ph/9703373].

12. M. V. Polyakov and A. Rathke, Eur. Phys. J. A **18**, 691 (2003) [arXiv:hep-ph/0303138].

13. D. Diakonov and V. Petrov, Phys. Rev. D **69**, 094011 (2004) [arXiv:hep-ph/0310212].

14. I. Jaegle [CBELSA-TAPS Collaboration], *Prepared for International Workshop on the Physics of Excited Baryons (NSTAR 05), Tallahassee, Florida, 10-15 Oct 2005*

15. A. Hosaka, contribution to Baryon07, Seoul, Korea, unpublished.

16. K. S. Choi, S. i. Nam, A. Hosaka and H. C. Kim, Phys. Lett. B **636** (2006) 253.

17. V. Shklyar, H. Lenske and U. Mosel, Phys. Lett. B **650** (2007) 172.

18. A. Fix, L. Tiator and M. V. Polyakov, Eur. Phys. J. A **32** (2007) 311.

19. I. Jaegle *et al.*, Phys. Rev. Lett. **100** (2008) 252002.

20. R. A. Arndt, I. I. Strakovsky and R. L. Workman, Phys. Rev. C **53**, 430 (1996) [arXiv:nucl-th/9509005].

21. B. Krusche *et al.*, Phys. Lett. B **358** (1995) 40.

22. A. Fantini *et al.*, Phys. Rev. C **78**, 015203 (2008).

23. P. Levi Sandri *et al.* [GRAAL Collaboration], Int. J. Mod. Phys. A **22** (2007) 341.

24. U. Thoma *et al.* (The CB-ELSA Collaboration), Phys. Lett. B **659** (2008) 87.

25. A. V. Sarantsev *et al.* (The CB-ELSA Collaboration), Phys. Lett. B **659** (2008) 94.

26. A. V. Anisovich, V. Kleber, E. Klempt, V. A. Nikonov, A. V. Sarantsev and U. Thoma, Eur. Phys. J. A **34** (2007) 243.

27. V. A. Nikonov, A. V. Anisovich, E. Klempt, A. V. Sarantsev and U. Thoma, Phys. Lett. B **662** (2008) 245.

28. I. Horn *et al.* (The CB-ELSA Collaboration), in preparation for Eur. Phys. J. A.

29. M. Lacombe, B. Loiseau, R. Vinh Mau, J. Cote, P. Pires and R. de Tourreil, Phys. Lett. B **101** (1981) 139.

30. V. V. Anisovich, M. N. Kobrinsky, D. I. Melikhov and A. V. Sarantsev, Nucl. Phys. A **544** (1992) 747.

31. O. Bartholomy *et al.* [CB-ELSA Collaboration], Eur. Phys. J. A **33** (2007) 133.

32. R.A. Arndt *et al.*, http://gwdac.phys.gwu.edu.

33. R. A. Arndt, W. J. Briscoe, I. I. Strakovsky and R. L. Workman, Phys. Rev. C **74** (2006) 045205.

34. R. A. Arndt, I. I. Strakovsky, R. L. Workman and M. M. Pavan, Phys. Rev. C **52** (1995) 2120 [arXiv:nucl-th/9505040].

35. A. V. Anisovich and A. V. Sarantsev, Eur. Phys. J. A **30** (2006) 427 [arXiv:hep-ph/0605135].

36. S. Prakhov *et al.*, Phys. Rev. C **72** (2005) 015203.

37. W. B. Richards *et al.*, Phys. Rev. D **1**, 10 (1970).

38. A. V. Anisovich, contribution to NSTAR 2007, Bonn, Germany, unpublished.

39. A. V. Anisovich, A. Sarantsev, O. Bartholomy, E. Klempt, V. A. Nikonov and U. Thoma, Eur. Phys. J. A **25** (2005) 427.

40. A. V. Sarantsev, V. A. Nikonov, A. V. Anisovich, E. Klempt and U. Thoma, Eur. Phys. J. A **25** (2005) 441.

41. V. Kuznetsov and M. V. Polyakov, arXiv:0807.3217 [hep-ph].

42. Y. I. Azimov, V. Kuznetsov, M. V. Polyakov and I. Strakovsky, Eur. Phys. J. A **25** (2005) 325 [arXiv:hep-ph/0506236].

43. O. Bartalini *et al.* [The GRAAL collaboration], Eur. Phys. J. A **33** (2007) 169.

44. W. M. Yao *et al.* [Particle Data Group], J. Phys. G **33** (2006) 1.

45. N. Awaji *et al.*, DPNU-29-81, Aug 1981. 11pp. Contributed paper to 10th Int. Symp. on Lepton and Photon Interactions at High Energy, Bonn, West Germany, Aug 24-28, 1981.

46. K. Fujii *et al.*, Nucl. Phys. B **187**, 53 (1981).

47. I. Arai, *In *Toronto 1980, Proceedings, Baryon 1980*, 93-105*

48. R. L. Crawford, *In *Toronto 1980, Proceedings, Baryon 1980*, 107-112*

49. W. T. Chiang, S. N. Yang, L. Tiator, M. Vanderhaeghen and D. Drechsel, Phys. Rev. C **68** (2003) 045202 [arXiv:nucl-th/0212106].

50. R. Koniuk and N. Isgur, Phys. Rev. **D21**, (1980) 1868.

51. Z. Li and F.E. Close, Phys. Rev. **D42**, (1990) 2207.

52. R. Bijker, F. Iachello and A. Leviatan, Ann. Phys. **236**, (1994) 69.

53. S. Capstick, Phys. Rev. **D46**, (1992) 2864.